

# 360BEV: Panoramic Semantic Mapping for Indoor Bird's-Eye View

Zhifeng Teng<sup>1,\*</sup>, Jiaming Zhang<sup>1,\*;†</sup>, Kailun Yang<sup>2</sup>, Kunyu Peng<sup>1</sup>,  
Hao Shi<sup>3</sup>, Simon Reiß<sup>1</sup>, Ke Cao<sup>1</sup>, Rainer Stiefelhagen<sup>1</sup>

<sup>1</sup>Karlsruhe Institute of Technology, <sup>2</sup>Hunan University, <sup>3</sup>Zhejiang University

## Abstract

Seeing only a tiny part of the whole is not knowing the full circumstance. Bird's-eye-view (BEV) perception, a process of obtaining allocentric maps from egocentric views, is restricted when using a narrow Field of View (FoV) alone. In this work, mapping from 360° panoramas to BEV semantics, the **360BEV** task, is established for the first time to achieve holistic representations of indoor scenes in a top-down view. Instead of relying on narrow-FoV image sequences, a panoramic image with depth information is sufficient to generate a holistic BEV semantic map. To benchmark 360BEV, we present two indoor datasets, 360BEV-Matterport and 360BEV-Stanford, both of which include egocentric panoramic images and semantic segmentation labels, as well as allocentric semantic maps. Besides delving deep into different mapping paradigms, we propose a dedicated solution for panoramic semantic mapping, namely **360Mapper**. Through extensive experiments, our methods achieve 44.32% and 45.78% in mIoU on both datasets respectively, surpassing previous counterparts with gains of +7.60% and +9.70% in mIoU.<sup>1</sup>

## 1. Introduction

Semantic scene understanding has achieved remarkable performance on indoor- and outdoor scenes via pixel-wise semantic segmentation [22]. It can be utilized directly on a wide range of downstream applications, such as autonomous driving [9, 12], navigation in robotics [3, 5] or in assistive technologies [38] to name a few. Recently, Bird's-Eye-View (BEV) semantic perception [16] can be a solution for enabling a straightforward understanding of the environment and objects therein. While BEV semantic segmentation has gained traction in outdoor scenes for autonomous driving [16], BEV perception has not yet been extensively explored for indoor scenes, which are often characterized

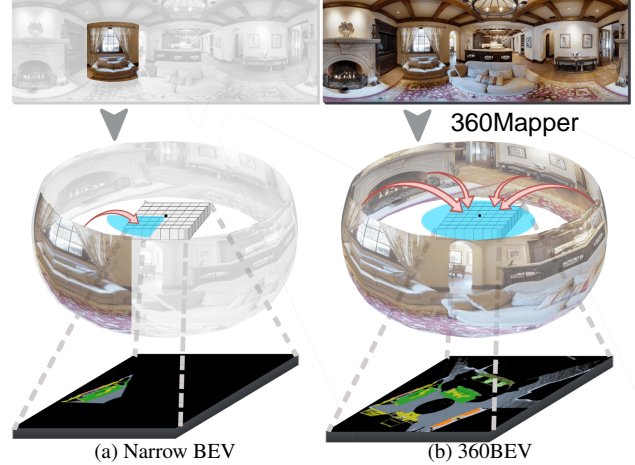


Figure 1. Semantic mapping from egocentric front-view images to allocentric BEV semantics. While (a) the narrow-BEV method has limited perception and map range, (b) 360BEV has an omni-directional Field of View, yielding a more complete BEV map by using our 360Mapper model.

by complex and varied structures, objects, and challenging lighting conditions. For semantically mapping these indoor scenes, sequence-based methods [3, 5] were proposed, which have to process whole videos and entail a moving camera. As shown in Fig. 1a, (1) these methods rely on computationally expensive processing of entire sequences of video-frames due to the narrow Field of View of the pin-hole camera, and (2) they are constrained to explore indoor mapping on synthetic simulators [26, 33], due to the lack of real indoor datasets. These drawbacks limit their applicability to real-world indoor semantic mapping.

To solve these limitations, in this work we introduce **360BEV** to achieve panoramic semantic mapping for indoor BEV, which is illustrated in Fig. 1b. Our considerations are twofold: (1) To unleash the potential of indoor semantic mapping in real-world scenarios, real indoor databases with BEV semantic labels are crucial and (2) to reduce computational complexity of narrow-FoV sequence methods [3] (more than 20 video-frames to process) or the complexity of multi-camera setups [16] (over 6 camera views needed) we leverage a single-frame 360°

\*Equal contribution.

†Corresponding author (e-mail: jiaming.zhang@kit.edu).

<sup>1</sup>The presented datasets and our code will be made publicly available at: <https://jamycheung.github.io/360BEV.html>.

image and thus bypass multi-sensor calibration, synchronization, and data fusion procedures. With this in mind and to enable 360BEV segmentation we present two real indoor BEV datasets, which are extended from the Matterport3D [4] and Stanford2D3D [2] datasets. First, the Front-View images captured by pinhole cameras from Matterport3D are extended to 360° panoramas for benchmarking on **360FV-Matterport**. Furthermore, to enable bird’s-eye view mapping, two BEV datasets, **360BEV-Matterport** and **360BEV-Stanford** are established by transforming front-view semantic labels to top-down views. These two datasets pave the way to – for the first time – predicting a complete BEV semantic map from a single-frame 360° image. Moreover, by decoupling the computationally expensive processing of sequences or multiple views, our direct 360BEV semantic mapping is more streamlined for generating indoor semantic maps.

Spatial distortions and object deformations in panoramic images [39] severely harm the performance of methods proposed for narrow-range image [11, 34] or multi-view perception [16]. Thus, to comprehensively investigate the established 360BEV task, we first revisit possible projection paradigms for 360BEV, including: (1) *Early projection* (2) *Late projection* and (3) *Intermediate projection*. Based on our observation that intermediate features maintain dense information, we explore the intermediate projection paradigm and propose a dedicated solution for 360BEV mapping, which we call **360Mapper**. The challenge in this scheme resides in the feature conversion. While the prior BEVFormer [16] relied on multi-view perception and SM-Net [3] projects the extracted feature directly via the depth-based transformation index, which are not appropriate for panoramic imagery due to its distortions and deformations, we propose a new transformation method, the **Inverse Radial Projection (IRP)**, to project features from 2D to 3D representations using only depth information. An additional benefit is that the depth information helps maintain object shape and space layout after being transferred to top-down views, rendering the 2D reference index for feature map as well as the BEV representation more accurate and consistent. Besides, unlike the deformable attention [16, 45] using multi-scale layers and fusion from multi-view cameras, we adopt **360Attention** with adaptive sampling offsets to extract information on a single panoramic feature map, yielding the bird’s-eye-view feature with less distortion in an adaptive manner. These are combined with the 2D index obtained by IRP to include a deformation-aware mechanism in 360 scenes, which in turn serves to compensate for the adverse effects of distortion. With these designs, our 360Mapper model represents a step towards a more complete and accurate indoor semantic mapping, which has important implications for down-stream applications such as indoor navigation and scene understanding.

Through extensive experiments the new 360BEV task is thoroughly benchmarked with two real indoor BEV datasets, three projection paradigms, and more than ten methods, respectively. Compared to the semantic mapping counterparts, our 360Mapper models achieve state-of-the-art performance, with mean intersection-over-union (mIoU) gains of over 7% on the 360BEV-Matterport dataset and over 9% on the 360BEV-Stanford dataset.

To summarize, we present the following contributions:

- A new *360BEV* task is introduced for the first time to address indoor semantic mapping via a single-frame panoramic image, bypassing complex multi-view perception and narrow-view sequence generation.
- Two real-world indoor BEV datasets, *i.e.*, *360BEV-Matterport* and *360BEV-Stanford*, are presented to include front-view panoramic images and BEV semantic labels, enabling end-to-end training.
- *360Mapper* – a dedicated solution for interior panoramic semantic mapping is proposed, exhibiting mIoU gains of over 7% as compared to the baseline.

## 2. Related Work

### 2.1. Panoramic Semantic Segmentation

Image semantic segmentation [31, 34, 36, 41] has achieved great progress. In contrast to narrow-FoV perception, panoramic semantic segmentation [6–8, 13, 29, 30, 37, 39], yielding holistic scene understanding by using a single 360° front-view image, has received increasing attention in recent years. In the field of indoor panorama segmentation, there are some benchmarks that provide synthetic [15, 42] and real [2] panoramic images and labels for training. Matterport3D [4] has large-scale panoramic images collected from 90 indoor buildings, yet, it has not been benchmarked due to the lack of corresponding semantic labels. To enable this, we generate the panoramic semantic segmentation labels through combining original 18 pinhole camera labels regarding their camera transformation matrices. Therefore, a 360° Front-View (FV) dataset, *360FV-Matterport*, with large-scale real indoor scenes, is provided to facilitate panoramic semantic segmentation. Besides, the 360FV-Matterport dataset is required to perform the late-projection paradigm of BEV semantic mapping.

### 2.2. BEV Semantic Mapping

Apart from front-view image semantic segmentation, some previous work explored top-view semantic segmentation, known as semantic mapping [5, 22] in indoor scenes and bird’s-eye-view semantic segmentation [16, 24] in outdoor driving scenes. The indoor semantic mapping methods can be divided into three categories according to the level of projection from the front view to the top-down view: *Early-projection* approaches [20, 28] are performed

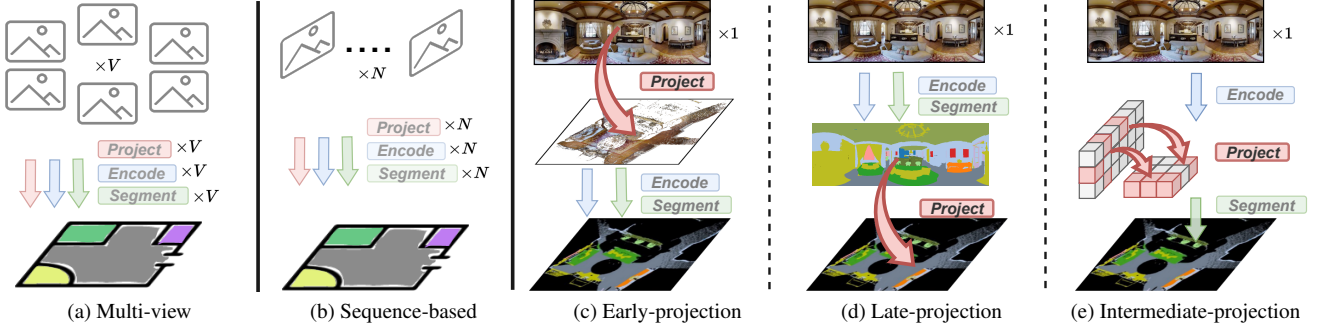


Figure 2. **Paradigms of semantic mapping.** While the narrow-FoV (a) multi-view and (b) sequence-based methods rely on  $V \geq 6$  and  $N \geq 20$  views, the 360°-BEV (c) Early-, (d) Late-, and (e) Intermediate-projection methods use a single panorama.

via general semantic segmentation methods, which first construct the BEV views from perspective images and then apply segmentation. Unfortunately, these pipelines lose fine-grained visual cues during the projection and thus result in unsatisfactory performance for small object segmentation. *Intermediate-projection* methods [3, 5] directly take front views as input for holistic indoor scene understanding, however, they work on synthetic data generated from Gibson [33] or Habitat [26] simulators, and rely on time-consuming image sequences. For example, SMNet [3] gradually captures an average of 2,500 view-points for each floor to generate a semantic map for indoor scenes. Instead, we explore to achieve efficient allocentric scene understanding via a single panorama image. The *Late-projection* pipeline [1, 10, 21, 25, 27] performs egocentric semantic segmentation and project labels to top-down views, which are sensitive to depth map and agent pose information, inevitably facing the projection error and under-fitting of model training, thus remaining a suboptimal solution. There are some BEV-related methods which leverage multiple perspective view sensors or LiDAR sensors and focus on outdoor object detection [17, 18, 35], optical flow estimation [14, 19], and semantic segmentation [23, 44]. Different from previous methods, our 360Mapper is carefully designed for learning indoor holistic representations by forwarding a single panorama without using multi-view images, image sequences, or point clouds.

### 3. Panorama Semantic Mapping (360BEV)

To investigate the 360BEV task, we analyze potential panoramic projection paradigms in Sec. 3.1. The generation and data statistic of the dataset are detailed in Sec. 3.2. To tackle the challenging panoramic semantic mapping, in Sec. 3.3 we present our solution **360Mapper** with the **Inverse Radial Projection** method and **360Attention** module, which enable distortion-aware feature processing.

#### 3.1. 360 Projection Paradigms

As shown in Fig. 2, unlike multi-view methods relying on more than six views  $V$  (Fig. 2a) and sequence-based methods using more than 20 narrow views  $N$  (Fig. 2b), panoramic semantic mapping uses a single image. We investigate the latter scenario with three projection paradigms, *i.e.*, how to process data from front-view panoramas to birds'-eye-view semantics, which are:

- (1) *Early projection*: **Proj.**  $\rightarrow$  **Enc.**  $\rightarrow$  **Seg.** in Fig. 2c. This way of processing might harm the original visual information and the spatial relationship of indoor objects, leading to lower performance of semantic mapping.
- (2) *Late projection*: **Enc.**  $\rightarrow$  **Seg.**  $\rightarrow$  **Proj.** in Fig. 2d. The front-view segmentation errors caused by distortion and deformation of panoramas accumulate and affect the completeness of object masks in the BEV map.
- (3) *Intermediate projection*: **Enc.**  $\rightarrow$  **Proj.**  $\rightarrow$  **Seg.** in Fig. 2e. In this manner, the encoded feature maintains dense and representative information, which is crucial for view projection. Besides, the projected features are further parsed by the subsequent BEV decoder.

Based on these properties, we mainly explore 360BEV with intermediate projections, in which we identify the following challenges: In the feature extraction stage, spatial distortions and object deformations severely hinder the encoder from extracting representative features from the front-view panoramic image. For the intermediate feature projection, only depth information is utilized to consistent view transformation of high-dimensional features. In addition, many large objects in the front view (*e.g.*, walls) are projected to thin objects in the top-down view, which greatly impedes capturing wide-range features during projection.

#### 3.2. 360FV and 360BEV Datasets

To benchmark the proposed 360FV and 360BEV tasks, in addition to the extended *360FV-Matterport* dataset for Front-View (FV) panoramic semantic segmentation, two Bird's-Eye-View (BEV) datasets, *i.e.*, *360BEV-Matterport*

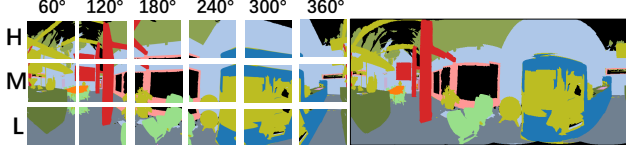


Figure 3. **360FV semantics generation** from 18 narrow (60°) views to a panoramic (360°) view on the 360FV-Matterport dataset. *H*, *M*, *L* represent high, medium, and low positions, respectively.

and *360BEV-Stanford*, are put forward for top-down panoramic semantic mapping.

**360FV-Matterport.** Compared to Stanford2D3D, which was sampled on the campus, Matterport3D [4] was collected from 90 residential buildings with diverse indoor scenes. As shown in Fig. 3, we convert the 18 annotations in the multiple narrow FoV images into a single 360° semantic ground truth, according to the corresponding rotation-translation matrices. As a result, our data processing yields in total 10,800 panoramic semantic labels for front-view panoramic semantic segmentation. We believe that such a front-view dataset with multiple complex scenes and diverse object categories can also foster progress in panoramic semantic segmentation.

**360BEV-Stanford.** The Stanford2D3D dataset [2] contains 1,413 panoramic images, along with the corresponding depths, semantic annotations, and panoramic global XYZ images, where each pixel in panoramic images corresponds to an identified  $(x, y, z)$  coordinate. As presented in Fig. 4, we can obtain spatial semantic information regarding the corresponding global XYZ image. Based on that, we generate 1,413 BEV semantic images with 13 annotated categories within a visible range as our ground truth by applying orthographic projection from generated spatial semantics. Unlike the projection method in SMNet [3], where the challenging objects are removed due to accumulated errors in time series, *i.e.*, *wall*, *door*, *window*, and *floor* classes, our single-frame method can accurately preserve them in our 360BEV dataset, as they are crucial for downstream indoor tasks, *e.g.*, robot navigation.

**360BEV-Matterport.** The Matterport3D dataset [4] does not provide the global XYZ modality as Stanford2D3D. Further, the method of generating BEV semantic ground truth from 3D annotated meshes according to dividing room blocks cannot reflect the ability of the panoramic view to cope with flexible scenarios such as crossing bedroom and toilet, hallway and living room. Inspired by the global XYZ modality [2], we generate a global XYZ for each panoramic image by using the provided depth ground truth. In order to generate BEV semantic ground truth corresponding to the panoramic view, several key steps must be considered. Firstly, a panoramic image can be processed as a sphere with rays shooting from the centre of the sphere, where the

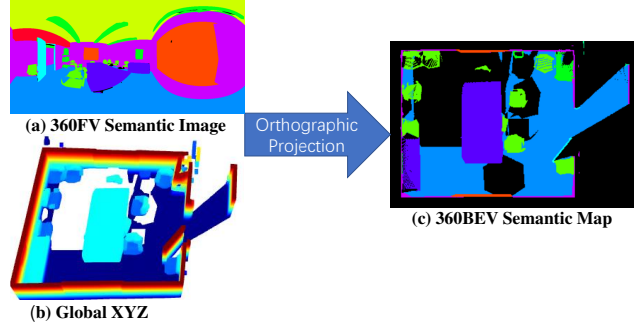


Figure 4. **360BEV semantics generation** by orthographic projection, from (a) the front-view semantic image and (b) the global XYZ image, to (c) the 360BEV semantic map.

camera is located. The image pixel  $(i, j)$  can be transformed here into the spherical coordinate system, as depicted in Eq. (1), representing as  $\Theta$ , and  $\Phi$ .

$$\begin{aligned}\Theta_{i,j} &= \frac{i\pi}{H} + \frac{\pi}{2H}, \\ i &= \{0, \dots, H-1\}, j = \{0, \dots, W-1\}, \\ \Phi_{i,j} &= -\frac{2\pi j}{W} + \pi - \frac{\pi}{W}, \\ i &= \{0, \dots, H-1\}, j = \{0, \dots, W-1\},\end{aligned}\quad (1)$$

Here,  $\Theta$  and  $\Phi$  are angle matrices of panoramic images with size  $H \times W$ , which consist of two dimensional Euler angular equivariant series. Given the representation in spherical coordinate systems, each 3D point  $(X_{i,j}, Y_{i,j}, Z_{i,j})$  in the camera coordinate system will be obtained through the calculation in Eq. (2),

$$\begin{aligned}X_{i,j} &= D_{i,j} \cdot \sin(\Theta_{i,j}) \cdot \sin(\Phi_{i,j}), \\ Y_{i,j} &= D_{i,j} \cdot \cos(\Theta_{i,j}), \\ Z_{i,j} &= D_{i,j} \cdot \sin(\Theta_{i,j}) \cdot \cos(\Phi_{i,j}),\end{aligned}\quad (2)$$

where  $D$  is the panoramic depth information. After obtaining 3D points, the orthographic projection matrix  $P_v$  is applied to transform 3D coordinates to 2D panoramic BEV indices  $(u, v)$ , which is presented in Eq. (3), where  $[\mathbf{R}|\mathbf{t}]$  is the transformation matrix.

$$\begin{aligned}\begin{bmatrix} x \\ y \\ z \end{bmatrix} &= \mathbf{R}^{-1} \begin{bmatrix} X_{i,j} \\ Y_{i,j} \\ Z_{i,j} \end{bmatrix} - \mathbf{t}, \\ \underbrace{\begin{bmatrix} u \\ v \\ 0 \\ 1 \end{bmatrix}}_{\text{Orthographic projection}} &= P_v \begin{bmatrix} x \\ y \\ z \\ 1 \end{bmatrix}.\end{aligned}\quad (3)$$

**Dataset statistics.** After data transformation, two BEV datasets for panoramic semantic mapping are obtained.



Table 1. **The data statistics** of 360BEV-Matterport and 360BEV-Stanford datasets.

Dataset	#Scene	#Room	#Frame	#Category
train	5	215	1,040	13
val	1	55	373	13
360BEV-Stanford	6	270	1,413	13
train	61	—	7,829	20
val	7	—	772	20
test	18	—	2,014	20
360BEV-Matterport	86	2,030	10,615	20

The overall statistical information of the two datasets is shown in Table 1. The Matterport3D dataset [4] consists of reconstructed 3D meshes of 90 indoor environments, such as homes, offices, and churches. There are 40 object categories in the dense annotation. However, many of them are relatively rare in the original dataset, *e.g.*, *TV* and *beam* ( $\ll 0.1\%$ ), which are excluded. Nonetheless, in order to produce dense BEV semantic map, we keep classes such as *walls* and *doors* which appear as thin lines and which are especially challenging in BEV tasks. Thus, 360BEV-Matterport maintains the 20 most common object categories and merges some uncommon classes, ranked by the number of object instances: wall, floor, chair, door, table, picture, furniture, objects, window, sofa, bed, sink, stairs, ceiling, toilet, mirror, shower, bathtub, counter, and shelving. The 360BEV-Matterport dataset is divided into three subsets, consisting of 61 scenes for training, 7 scenes for validation, and 18 scenes for testing. Besides, we further calculate the per-class pixel number and per-class frequency of both BEV datasets in Fig. 5. It is worth noting that the *floor* class has a much higher frequency on both datasets. This category is important for tasks that rely on complete maps, such indoor navigation and is therefore also retained.

### 3.3. Proposed Model: 360Mapper

**Overall Architecture.** After introducing the 360BEV task and datasets, in this section, we describe our **360Mapper** model, which considers the paradigm of intermediate projection. As shown in Fig. 6, our end-to-end 360Mapper framework includes four steps: (1) The panoramic images are fed into the transformer-based backbone, which extracts contextual features from the front view. (2) The **Inverse Radial Projection (IRP)** module obtains a 2D index by projecting reference points which are generated by panoramic depth images. (3) The **360Attention** module enhances the feature from the front-view encoder by using the index from IRP and generates offsets from BEV queries to eliminate the effects of distortion. (4) The lightweight decoder parses the projected feature map and predicts the se-

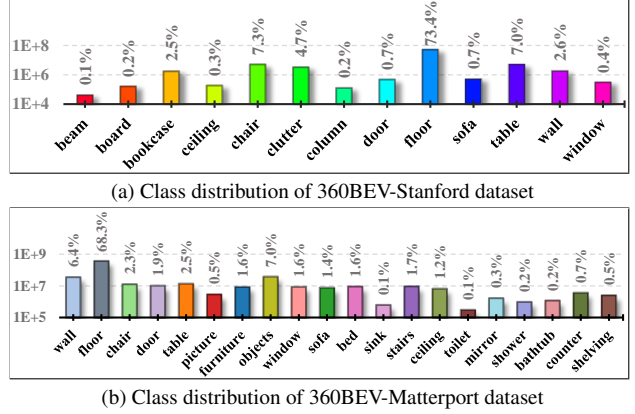


Figure 5. **Per-class pixel number (logarithmic) and frequency (%) distribution** of two 360BEV datasets.

mantic maps in top-down view.

**Inverse Radial Projection.** Next, we propose a flexible projection method, the Inverse Radial Projection (IRP), for which the input of panoramic depth is included. We can easily obtain a top-view mask map by projecting from depth information. This mask map is then used to generate 3D reference points with the corresponding map height. 3D reference points are projected onto the sphere to generate 2D reference indexes, as shown in Eq. (4), where  $ID_h$  and  $ID_w$  represent the index values of the 2D reference for the height and width of the feature map, respectively. The 2D reference indexes are then used to locate the corresponding feature points on the encoded front-view feature map.

$$\begin{aligned}
 \Phi &= \tan^{-1} \frac{y}{x}, \\
 \Theta &= \tan^{-1} \left( \frac{x}{z} \cdot \frac{1}{\cos(\Phi)} \right), \\
 ID_h &= \left\lceil \frac{H\Theta}{\pi} \right\rceil, \\
 ID_w &= \left\lceil \left( \frac{\Phi}{\pi} - \frac{1}{W} \right) \cdot \frac{W}{2} \right\rceil.
 \end{aligned} \tag{4}$$

Due to the distortions in the stitching process of the panorama, it is hard to project the 3D reference points exactly onto the 2D front-view plane by rotation and translation. Thus, we use the depth map to generate a map mask that better describes the shape of the map, so that the accurate projection with the mask not only makes the amount of data entering the 360Attention much smaller, which is conducive to the fast convergence of the model, but also facilitates the use of sampling offsets for 360Attention.

**360Attention.** In Fig. 6b, the proposed 360Attention generates sampling offsets through the linear layer in an adaptive manner. Given the BEV query  $q \in \mathbb{R}^{N \times C_{Emb}}$  as input, where  $N=h \times w$  is the length of query, a *mask*( $\cdot$ ) operation is applied on  $q$  and  $p$  to mask out irrelevant points

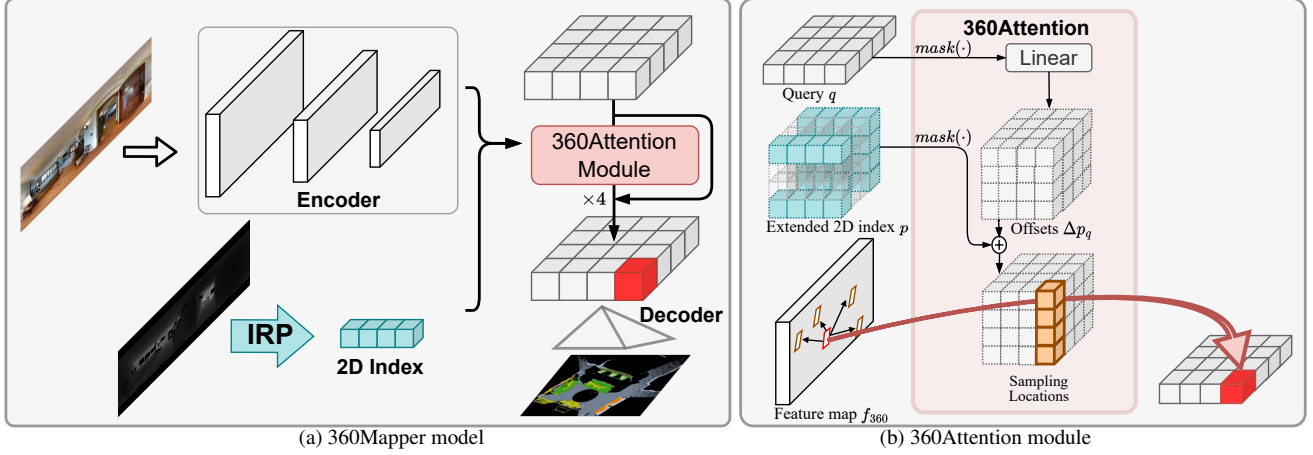


Figure 6. **Architecture of 360Mapper and the 360Attention module.** The 360Mapper model includes the encoder for extracting features from the front-view panoramic image, the 360Attention module for feature projection, and the decoder for parsing the projected feature to the BEV semantic map. The offsets are obtained by a linear layer and added with the 2D index that is obtained by Inverse Radial Projection (IRP), yielding the sampling locations for 360BEV feature projection.

and 2D indexes according to the mask map  $M_{map}$  from IRP, which is crucial to keep  $q$  and  $p$  efficient and reducing computation of 360Attention ( $\sum M_{map} < N$ ). The sampling offset  $\Delta p_{q,ij}$  and attention weight  $\mathcal{A}_{ij} \in [0, 1]$  are predicted through BEV query by linear layers respectively. The adaptive sampling offsets are then added to the extended 2D index  $p$  to obtain distortion-aware sampling locations. The 360Attention module can be denoted as:

$$360Attn(q, p, f_{360}) = \sum_{i=1}^{N_{head}} \mathcal{W}_i \sum_{j=1}^{N_{point}} \mathcal{A}_{ij} \cdot f_{360} (mask(p) + \Delta p_{q,ij}), \quad (5)$$

where  $q$ ,  $p$ , and  $f_{360}$  indicate the query, the extended 2D index, and panoramic feature map, respectively. The linear layer  $\mathcal{W}_i \in \mathbb{R}^{C \times (C/N_{head})}$  is specific to each attention head  $i$ , where  $C$  is the feature dimension and  $N_{head}$  is the number of heads. The attention weight  $\mathcal{A}_{ij}$  represents the importance of the sampled points  $j$ , where  $\sum \mathcal{A}_{ij} = 1$ . The panoramic features  $f_{360}$  and the adaptive sampling locations  $(mask(p) + \Delta p_{q,ij})$  are aggregated using attention weights  $\mathcal{A}_{ij}$  to produce a BEV output. Afterwards, the mask map  $M_{map}$  is applied to assemble the BEV output as  $q' \in \mathbb{R}^{N \times C_{Emb}}$ . After added a residual term of  $q$ , the BEV result  $q + q'$  is forwarded to the next 360Attention module.

Compared to Spatial Cross-Attention module in BEVFormer [16], the difference lies in: (1) Instead of relying on multi-view features across multiple cameras, our 360Attention module is designed to directly adopt adaptive sampling offsets to extract feature from a single panoramic feature map. (2) Our module gets rid of the projection of 3D reference points to different image views using the projection matrix, thus compensating for the lack of front-view perception. (3) The mask operation is applied to maintain the

BEV query efficient and adaptive to front-view panoramic features by using depth information as a bridge. Through these non-trivial designs, the BEV feature map generated by 360Attention is able to effectively neutralise the effects of front-view distortion.

## 4. Experiments

### 4.1. Implementation Details

We train 360Mapper models with 4 A100 GPUs with an initial learning rate of  $6e^{-5}$ , scheduled by the step strategy over 50 epochs. AdamW is the optimizer with epsilon  $1e^{-8}$ , weight decay is 0.01 and batch size is 4 on each GPU. The panoramic image size of 360FV-Matterport and Stanford2D3D [2] are both  $512 \times 1024$ . The resolution of panoramic images on both 360BEV-Stanford and 360BEV-Matterport datasets are  $512 \times 1024$  as input for 360Mapper training, while the output BEV maps are set to  $500 \times 500$ , which correspond to a perception range of  $10m \times 10m$ . Following [3, 5], evaluation metrics are pixel-wise accuracy (Acc), pixel recall (mRecall), precision (mPrecision), and mean Intersection-over-Union (mIoU).

### 4.2. Panorama Semantic Segmentation (360FV)

**Results on Stanford2D3D.** The front-view panoramic semantic segmentation results on Stanford2D3D dataset are presented in Table 2. All results are averaged over 3 cross validation folds. Thanks to the proposed 360Attention module, our 360Mapper model is better capable of handling deformations in panoramas, yielding 54.3% in mIoU, with  $>2\%$  performance gains as compared to the previous state-of-the-art Trans4PASS [39] and CFCB [43]. The promising result in front-view panoramas has initially revealed the po-

Table 2. **Panoramic semantic segmentation (360FV)** on the Stanford2D3D dataset.

Method	Backbone	Input	mIoU(%)
Tangent [7]	ResNet-101	RGB	45.6
SegFormer [34]	MiT-B2	RGB	51.9
HoHoNet [29]	ResNet-101	RGB	52.0
Trans4PASS [39]	MiT-B2	RGB	52.1
CFCB [43]	ResNet-101	RGB	52.2
Ours	MiT-B2	RGB	<b>54.3</b>

Table 3. **Panoramic semantic segmentation (360FV)** on the val set of 360FV-Matterport dataset.

Method	Backbone	Input	mIoU(%)
HoHoNet [29]	ResNet-101	RGB	44.10
HoHoNet [29]	ResNet-101	RGB-D	44.85
Trans4PASS [39]	MiT-B2	RGB	41.91
Trans4PASS+ [40]	MiT-B2	RGB	42.60
SegFormer [34]	MiT-B2	RGB	45.53
Ours	MiT-B2	RGB	<b>46.35</b>

tential of our model in extracting 360° front-view features, which is crucial for the BEV semantic mapping task as well. **Results on 360FV-Matterport.** Due to the limited amount of data on Stanford2D3D, for the first time, a large-scale benchmark, 360FV-Matterport, is brought to the community of front-view panoramic semantic segmentation. To conduct a comprehensively comparison on this new benchmark, in Table 3, four state-of-the-art methods are selected and reproduced. Compared to the Trans4PASS [39] and Trans4PASS+ [40] models, our model has respective +4.44% and +3.75% improvements. Furthermore, our model surpasses RGB-D HoHoNet [29] and SegFormer [34] with +1.50% and +0.82% mIoU gains. The results indicate that our model can consistently achieve the state-of-the-art performance on large-scale datasets for panoramic semantic segmentation.

### 4.3. Panorama Semantic Mapping (360BEV)

**Results on 360BEV-Stanford.** In Table 4, to study the Early projection mode, SegFormer [34] and SegNeXt [11] with different backbones, are selected, which merely reach unsatisfactory results. The results indicate that the pre-projected RGB maintains less rich spatial and visual information of front-view images. Using Late projection, SegFormer with the same MiT-B2 backbone achieves 18.65% mIoU and surpasses the one using Early projection, still yielding sub optimal semantic mapping results. Interestingly, all methods using Intermediate projection obtain more than 30% mIoU. While using the same MiT-B2 backbone and our proposed 360Mapper achieves 45.78% with +9.70% gains compared to the baseline Trans4Map [5]. Further, our efficient model (MiT-B0) outperforms Trans4Map (MiT-B4) with +05.73% mIoU gains. With a stronger CNN backbone MSCA-B from Seg-

Table 4. **Panoramic semantic mapping (360BEV)** on the 360BEV-Stanford dataset.

Method	Backbone	Acc	mRecall	mPrecision	mIoU
<i>(1) Early projection: Proj.→Enc.→Seg.</i>					
SegFormer [34]	MiT-B2	71.69	20.82	26.34	14.15
SegNeXt [11]	MSCA-B	79.77	34.13	47.39	25.85
<i>(2) Late projection: Enc.→Seg.→Proj.</i>					
HoHoNet [29]	ResNet101	70.01	31.62	30.46	18.49
Trans4PASS [39]	MiT-B2	65.73	31.08	33.15	17.86
Trans4PASS+ [40]	MiT-B2	66.11	38.06	34.14	20.44
SegFormer [34]	MiT-B2	70.50	30.97	30.65	18.65
<i>(3) Intermediate projection: Enc.→Proj.→Seg.</i>					
BEVFormer [16]	MiT-B2	85.50	40.22	51.71	31.69
Trans4Map [5]	MiT-B0	86.41	40.45	57.47	32.26
Trans4Map [5]	MiT-B2	86.53	45.28	62.61	36.08
Trans4Map [5]	MiT-B4	86.99	46.18	58.19	36.69
Ours	MiT-B0	92.07	50.14	65.37	42.42 (+10.16)
Ours	MiT-B2	<b>92.80</b>	53.56	67.72	45.78 (+9.70)
Ours	MSCA-B	92.67	<b>55.02</b>	<b>68.02</b>	<b>46.44</b>

Table 5. **Panoramic semantic mapping (360BEV)** on the val set of 360BEV-Matterport dataset.

Method	Backbone	Acc	mRecall	mPrecision	mIoU
<i>(1) Early projection: Proj.→Enc.→Seg.</i>					
SegFormer [34]	MiT-B2	68.12	41.33	45.25	29.22
SegNeXt [11]	MSCA-B	68.53	42.13	46.12	30.01
<i>(2) Late projection: Enc.→Seg.→Proj.</i>					
HoHoNet [29]	ResNet101	62.84	38.99	44.22	26.21
Trans4PASS [39]	MiT-B2	55.99	29.59	40.91	20.07
Trans4PASS+ [40]	MiT-B2	57.89	32.75	40.93	21.58
SegFormer [34]	MiT-B2	62.98	41.84	45.30	27.78
<i>(3) Intermediate projection: Enc.→Proj.→Seg.</i>					
BEVFormer [16]	MiT-B2	72.99	43.61	51.70	32.51
Trans4Map [5]	MiT-B0	70.19	44.31	50.39	31.92
Trans4Map [5]	MiT-B2	73.28	51.60	53.02	36.72
Trans4Map [5]	MiT-B4	73.51	50.78	56.67	38.04
Ours	MiT-B0	75.44	48.80	56.01	36.98 (+5.06)
Ours	MiT-B2	78.80	59.54	59.97	44.32 (+7.60)
Ours	MSCA-B	<b>78.93</b>	<b>60.51</b>	<b>62.83</b>	<b>46.31</b>

NeXt [11], our method reaches the best score with 46.44% in mIoU, which indicates 360Mapper is flexible to both CNN- and Transformer-based backbones.

**Results on 360BEV-Matterport.** To investigate 360BEV on a large-scale dataset, in Table 5, we conduct the same experiments on the 360BEV-Matterport dataset. SegFormer [34] and SegNeXt [11] adopt Early projection and show better performance than the approaches which adopt Late projection. The reason for this is Late projection methods are constrained by their lower performance in front-view semantic segmentation, which affects the projected BEV semantic maps. In contrast, using Intermediate projection, our 360Mapper models based on two different model scales, *i.e.*, MiT-B0 and MiT-B2, show overall promising performance with 36.98% and 44.32% mIoU, respectively. Compared to the previous state-of-the-art

Table 6. Analysis of offset mechanisms in 360Attention and backbone variants on 360BEV-Matterport dataset.

Methods	Backbone	#Param	FLOPs	mIoU
① Ours (360Attention offset)	MiT-B0	04.60M	248.57G	36.98
② Ours (360Attention offset)	MiT-B2	26.30M	283.94G	44.32
③ Ours (360Attention offset)	MiT-B4	62.91M	341.34G	<b>45.53</b>
④ Ours (Multi-scale offset)	MiT-B2	26.43M	284.17G	43.65 (-0.67)
⑤ Ours (Fixed-range offset)	MiT-B2	26.30M	283.44G	43.28 (-1.04)
⑥ Ours (Separate offset)	MiT-B2	26.19M	279.18G	42.82 (-1.50)
⑦ Ours (360Attention offset)	MSCA-B	27.69M	274.59G	<b>46.31 (+1.99)</b>

Trans4Map [5] (MiT-B2), our approach with MiT-B2 has improvements by +5.52% in accuracy, +7.94% in mRecall, +6.95% in mPrecision, and +7.60% in mIoU. Surprisingly, our 360Mapper with MiT-B2 outperforms Trans4Map with MiT-B4 with +6.28% in mIoU. Besides, to compare multi-view methods, we reproduce BEVFormer [16] by using a single panorama instead of six views of pinhole cameras. Our 360Mapper outperforms BEVFormer (MiT-B2) with +11.81% mIoU. Furthermore, we verify the flexibility of 360Mapper by using a CNN-based MSCA-B backbone [11], which obtains the highest mIoU score with 46.31%. All results are in line with our observation that Intermediate projection can preserve dense visual cues and long-range information from front-view panoramas, and deliver more valuable context for BEV semantic mapping, leading to this superiority of 360Mapper, as compared to the other paradigms.

**Analysis of 360Attention.** To better understand 360Attention, we further conduct an analysis of the offset mechanisms in 360Attention and the backbone selection, in Table 6. First, in ①②③, we select three model scales, *i.e.*, MiT-B0, MiT-B2, and MiT-B4, to verify the effect of model capacity in 360Attention. The three models obtain good performance, showing that 360Attention has positive effects in different model scales. Besides, different offset schemes are compared among ②④⑤⑥, which are deformable, multi-scale, fixed-range, and separate offset. All of them have the same MiT-B2 backbone. Here, ② shows the superiority of deformable offset which has a better performance (44.32%). However, these comparable results prove that our 360Attention design is robust to offset mechanisms. Further, to analyze the effect of backbone selection, we choose transformer-based MiT-B2 [34] and CNN-based MSCA-B [11] as in ②⑦. A stronger backbone [11] shows a further improvement of mIoU (+1.99%), which shows the flexibility of our approach regarding the backbone variants.

#### 4.4. Qualitative Analysis

To analyze the predicted semantic maps, we visualise the results from the validation set of the 360BEV-Matterport dataset. In Fig. 7, from left to right are input images, re-

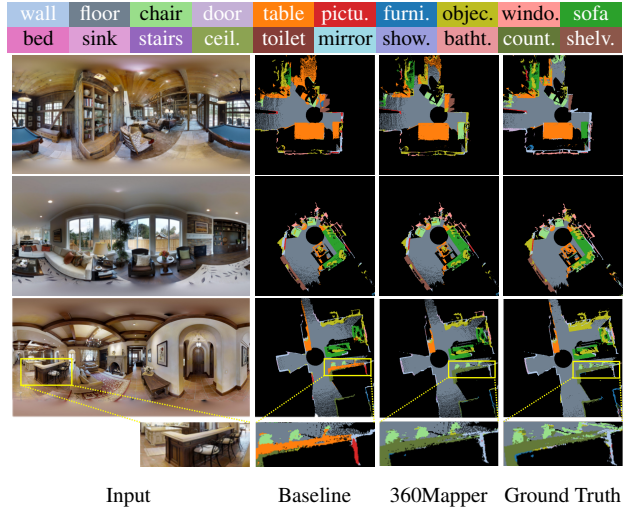


Figure 7. **Qualitative analysis** on the 360BEV-Matterport dataset. Black regions are void. Zoom-in for better view.

sults of baseline [5], results of our 360Mapper, and ground truth. Thanks to the IRP projection and 360Attention, the segmentation results of 360Mapper are much better. In the first scene in Fig. 7, 360Mapper is able to successfully classify *chairs*, while the baseline model fails, predicting several *tables* and misclassifying the distant ground as another *table*. In the second scene, the segmentation of the *tables* derived by the baseline is incomplete. Furthermore, in the last zoomed-in scene, 360Mapper provides accurate semantic maps, such as in *counter*, *chair*, and *wall* categories, whereas the baseline Trans4Map [5] misclassifies them as *tables* and *doors*. Based on the qualitative analysis, our 360Mapper can effectively handle object deformations and image distortions, yielding better BEV semantic maps.

## 5. Conclusion

In this paper, we introduce 360BEV, a new task to conduct panoramic semantic mapping in indoor scenes, *i.e.*, from a single panoramic image to a holistic BEV semantic map. To enable this, we present 360BEV-Matterport and 360BEV-Stanford, extending off-the-shelf datasets for the 360BEV task. We revisit existing transformation paradigms and propose 360Mapper, a novel end-to-end architecture specifically designed for panoramic semantic mapping. As a result, 360Mapper outperforms state-of-the-art counterparts by a clear margin.

**Limitations.** The 360BEV task is first investigated on indoor datasets. In future work, 360BEV on outdoor driving scenes will be explored. Using one panoramic camera to construct a holistic map has the potential to solve the bottleneck of sensor fusion and calibration caused by the multi-view BEV counterparts. Semantic scene completion is another promising direction, yielding semantic map anticipation beyond the visible range for downstream tasks.



## References

- [1] Peter Anderson, Qi Wu, Damien Teney, Jake Bruce, Mark Johnson, Niko Sünderhauf, Ian Reid, Stephen Gould, and Anton Van Den Hengel. Vision-and-language navigation: Interpreting visually-grounded navigation instructions in real environments. In *CVPR*, 2018. 3
- [2] Iro Armeni, Sasha Sax, Amir R. Zamir, and Silvio Savarese. Joint 2D-3D-semantic data for indoor scene understanding. *arXiv preprint arXiv:1702.01105*, 2017. 2, 4, 6, 11
- [3] Vincent Cartillier, Zhile Ren, Neha Jain, Stefan Lee, Irfan Essa, and Dhruv Batra. Semantic MapNet: Building allocentric semantic maps and representations from egocentric views. In *AAAI*, 2021. 1, 2, 3, 4, 6
- [4] Angel Chang, Angela Dai, Thomas Funkhouser, Maciej Halber, Matthias Niessner, Manolis Savva, Shuran Song, Andy Zeng, and Yinda Zhang. Matterport3D: Learning from RGB-D data in indoor environments. In *3DV*, 2017. 2, 4, 5, 11
- [5] Chang Chen, Jiaming Zhang, Kailun Yang, Kunyu Peng, and Rainer Stiefelham. Trans4Map: Revisiting holistic bird’s-eye-view mapping from egocentric images to allocentric semantics with vision transformers. In *WACV*, 2023. 1, 2, 3, 6, 7, 8, 11, 12, 13, 14, 15
- [6] Taco Cohen, Maurice Weiler, Berkay Kicanaoglu, and Max Welling. Gauge equivariant convolutional networks and the icosahedral CNN. In *ICML*, 2019. 2
- [7] Marc Eder, Mykhailo Shvets, John Lim, and Jan-Michael Frahm. Tangent images for mitigating spherical distortion. In *CVPR*, 2020. 2, 7
- [8] Carlos Esteves, Ameesh Makadia, and Kostas Daniilidis. Spin-weighted spherical CNNs. In *NeurIPS*, 2020. 2
- [9] Di Feng, Christian Haase-Schütz, Lars Rosenbaum, Heinz Hertlein, Claudius Glaeser, Fabian Timm, Werner Wiesbeck, and Klaus Dietmayer. Deep multi-modal object detection and semantic segmentation for autonomous driving: Datasets, methods, and challenges. *T-ITS*, 2020. 1
- [10] Margarita Grinvald, Fadri Furrer, Tonci Novkovic, Jen Jen Chung, Cesar Cadena, Roland Siegwart, and Juan Nieto. Volumetric instance-aware semantic mapping and 3d object discovery. *RA-L*, 2019. 3
- [11] Meng-Hao Guo, Cheng-Ze Lu, Qibin Hou, Zhengning Liu, Ming-Ming Cheng, and Shi-Min Hu. SegNeXt: Rethinking convolutional attention design for semantic segmentation. In *NeurIPS*, 2022. 2, 7, 8, 12, 13
- [12] Joel Janai, Fatma Güney, Aseem Behl, and Andreas Geiger. Computer vision for autonomous vehicles: Problems, datasets and state of the art. *Foundations and Trends® in Computer Graphics and Vision*, 2020. 1
- [13] Chiyu Max Jiang, Jingwei Huang, Karthik Kashinath, Prabhath, Philip Marcus, and Matthias Nießner. Spherical CNNs on unstructured grids. In *ICLR*, 2019. 2
- [14] Kuan-Hui Lee, Matthew Kliemann, Adrien Gaidon, Jie Li, Chao Fang, Sudeep Pillai, and Wolfram Burgard. PillarFlow: End-to-end birds-eye-view flow estimation for autonomous driving. In *IROS*, 2020. 3
- [15] Wenbin Li, Sajad Saeedi, John McCormac, Ronald Clark, Dimos Tzoumanikas, Qing Ye, Yuzhong Huang, Rui Tang, and Stefan Leutenegger. InteriorNet: Mega-scale multi-sensor photo-realistic indoor scenes dataset. In *BMVC*, 2018. 2
- [16] Zhiqi Li, Wenhai Wang, Hongyang Li, Enze Xie, Chonghao Sima, Tong Lu, Yu Qiao, and Jifeng Dai. BEVFormer: Learning bird’s-eye-view representation from multi-camera images via spatiotemporal transformers. In *ECCV*, 2022. 1, 2, 6, 7, 8, 13
- [17] Zhiqi Li, Wenhai Wang, Hongyang Li, Enze Xie, Chonghao Sima, Tong Lu, Yu Qiao, and Jifeng Dai. BEVFormer: Learning bird’s-eye-view representation from multi-camera images via spatiotemporal transformers. In *ECCV*, 2022. 3
- [18] Yingfei Liu, Tiancai Wang, Xiangyu Zhang, and Jian Sun. PETR: Position embedding transformation for multi-view 3D object detection. In *ECCV*, 2022. 3
- [19] Chenxu Luo, Xiaodong Yang, and Alan Yuille. Self-supervised pillar motion learning for autonomous driving. In *CVPR*, 2021. 3
- [20] Gellert Mattyus, Shenlong Wang, Sanja Fidler, and Raquel Urtasun. Enhancing road maps by parsing aerial images around the world. In *ICCV*, 2015. 2
- [21] Daniel Maturana, Po-Wei Chou, Masashi Uenoyama, and Sebastian Scherer. Real-time semantic mapping for autonomous off-road navigation. In *FSR*, 2018. 3
- [22] Branislav Mičušlák and Jana Košecká. Semantic segmentation of street scenes by superpixel co-occurrence and 3D geometry. In *ICCVW*, 2009. 1, 2
- [23] Bowen Pan, Jiankai Sun, Ho Yin Tiga Leung, Alex Andonian, and Bolei Zhou. Cross-view semantic segmentation for sensing surroundings. *RA-L*, 2020. 3
- [24] Lang Peng, Zhirong Chen, Zhangjie Fu, Pengpeng Liang, and Erkang Cheng. BEVSegFormer: Bird’s eye view semantic segmentation from arbitrary camera rigs. In *WACV*, 2023. 2
- [25] Teng Ran, Liang Yuan, Jianbo Zhang, Dingxin Tang, and Li He. RS-SLAM: A robust semantic SLAM in dynamic environments based on RGB-D sensor. *IEEE Sensors Journal*, 2021. 3
- [26] Manolis Savva, Jitendra Malik, Devi Parikh, Dhruv Batra, Abhishek Kadian, Oleksandr Maksymets, Yili Zhao, Erik Wijmans, Bhavana Jain, Julian Straub, Jia Liu, and Vladlen Koltun. Habitat: A platform for embodied AI research. In *CVPR*, 2019. 1, 3
- [27] Sunando Sengupta, Paul Sturgess, Lubor Ladicky, and Philip H. S. Torr. Automatic dense visual semantic mapping from street-level imagery. In *IROS*, 2012. 3
- [28] Suriya Singh, Anil Batra, Guan Pang, Lorenzo Torresani, Saikat Basu, Manohar Paluri, and C. V. Jawahar. Self-supervised feature learning for semantic segmentation of overhead imagery. In *BMVC*, 2018. 2
- [29] Cheng Sun, Min Sun, and Hwann-Tzong Chen. HoHoNet: 360 indoor holistic understanding with latent horizontal features. In *CVPR*, 2021. 2, 7, 11, 12, 13
- [30] Keisuke Tateno, Nassir Navab, and Federico Tombari. Distortion-aware convolutional filters for dense prediction in panoramic images. In *ECCV*, 2018. 2

- [31] Jingdong Wang, Ke Sun, Tianheng Cheng, Borui Jiang, Chaorui Deng, Yang Zhao, Dong Liu, Yadong Mu, Mingkui Tan, Xinggang Wang, Wenyu Liu, and Bin Xiao. Deep high-resolution representation learning for visual recognition. *TPAMI*, 2021. 2
- [32] Erik Wijmans, Samyak Datta, Oleksandr Maksymets, Abhishek Das, Georgia Gkioxari, Stefan Lee, Irfan Essa, Devi Parikh, and Dhruv Batra. Embodied question answering in photorealistic environments with point cloud perception. In *CVPR*, 2019. 11
- [33] Fei Xia, Amir R Zamir, Zhiyang He, Alexander Sax, Jitendra Malik, and Silvio Savarese. Gibson env: Real-world perception for embodied agents. In *CVPR*, 2018. 1, 3
- [34] Enze Xie, Wenhai Wang, Zhiding Yu, Anima Anandkumar, Jose M. Alvarez, and Ping Luo. SegFormer: Simple and efficient design for semantic segmentation with transformers. In *NeurIPS*, 2021. 2, 7, 8, 11, 12, 13
- [35] Chenyu Yang, Yuntao Chen, Hao Tian, Chenxin Tao, Xizhou Zhu, Zhaoxiang Zhang, Gao Huang, Hongyang Li, Yu Qiao, Lewei Lu, Jie Zhou, and Jifeng Dai. BEVFormer v2: Adapting modern image backbones to bird’s-eye-view recognition via perspective supervision. *arXiv preprint arXiv:2211.10439*, 2022. 3
- [36] Yuhui Yuan, Xilin Chen, and Jingdong Wang. Object-contextual representations for semantic segmentation. In *ECCV*, 2020. 2
- [37] Chao Zhang, Stephan Liwicki, William Smith, and Roberto Cipolla. Orientation-aware semantic segmentation on icosahedron spheres. In *ICCV*, 2019. 2
- [38] Jiaming Zhang, Kailun Yang, Angela Constantinescu, Kunyu Peng, Karin Müller, and Rainer Stiefelhagen. Trans4Trans: Efficient transformer for transparent object segmentation to help visually impaired people navigate in the real world. In *ICCVW*, 2021. 1
- [39] Jiaming Zhang, Kailun Yang, Chaoxiang Ma, Simon Reiß, Kunyu Peng, and Rainer Stiefelhagen. Bending reality: Distortion-aware transformers for adapting to panoramic semantic segmentation. In *CVPR*, 2022. 2, 6, 7, 11, 12, 13, 14
- [40] Jiaming Zhang, Kailun Yang, Hao Shi, Simon Reiß, Kunyu Peng, Chaoxiang Ma, Haodong Fu, Kaiwei Wang, and Rainer Stiefelhagen. Behind every domain there is a shift: Adapting distortion-aware vision transformers for panoramic semantic segmentation. *arXiv preprint arXiv:2207.11860*, 2022. 7, 11, 12, 13
- [41] Hengshuang Zhao, Jianping Shi, Xiaojuan Qi, Xiaogang Wang, and Jiaya Jia. Pyramid scene parsing network. In *CVPR*, 2017. 2
- [42] Jia Zheng, Junfei Zhang, Jing Li, Rui Tang, Shenghua Gao, and Zihan Zhou. Structured3D: A large photo-realistic dataset for structured 3D modeling. In *ECCV*, 2020. 2
- [43] Zishuo Zheng, Chunyu Lin, Lang Nie, Kang Liao, Zhijie Shen, and Yao Zhao. Complementary bi-directional feature compression for indoor 360deg semantic segmentation with self-distillation. In *WACV*, 2023. 6, 7
- [44] Brady Zhou and Philipp Krähenbühl. Cross-view transformers for real-time map-view semantic segmentation. In *CVPR*, 2022. 3
- [45] Xizhou Zhu, Weijie Su, Lewei Lu, Bin Li, Xiaogang Wang, and Jifeng Dai. Deformable DETR: Deformable transformers for end-to-end object detection. In *ICLR*, 2021. 2

## A. Data Generation

To perform the data generation, we use an open-source tool<sup>2</sup> to convert the 3D mesh semantic labels in Matterport3D [4] into 194,400 pinhole images with semantic labels. Then, every 18 semantic label pairs are concatenated via a corresponding rotation-translation matrix, yielding 10,800 panoramic semantic ground truth, which is referred to as 360FV-Matterport by us. These panoramic semantic images are originally annotated with 40 object categories. Because many of them are only a small percentage ( $\ll 0.1\%$ ), we merge some uncommon classes and maintain the 20 most common object categories: wall, floor, chair, door, table, picture, furniture, objects, window, sofa, bed, sink, stairs, ceiling, toilet, mirror, shower, bathtub, counter, and shelving. For another front-view semantic segmentation dataset, Stanford2D3D [2], we keep the original object classes: beam, board, bookcase, ceiling, chair, clutter, column, door, floor, sofa, table, wall, window.

For the presented 360BEV-Stanford dataset, we follow the data split method of Fold-1 of the Stanford2D3D [2] dataset. On the BEV dataset, we use the *area1*, *area2*, *area3*, *area4* and *area6* as the training data for the proposed 360BEV task, and we use the *area5a* and *area5b* as the validation set to evaluate the panoramic semantic mapping performance of models. The results of training and evaluation with the Fold-1 data split is similar the average scores which are calculated by using three-fold cross-validation. Besides, the validation set from Fold-1 is sufficient to evaluate the model performance on panoramic semantic mapping.

For 360BEV-Matterport, we use a different data split compared to Wijmans *et al.* [32]. Instead of using synthetic simulators, all samples on our dataset are converted from the real images and labels of Matterport3D [4] dataset, where there are 86 unique floors on our dataset, including 61 for training, 7 for validations, and 18 for testing.

## B. More Quantitative Analysis

### B.1. Results on Stanford2D3D

In Table 7, we present the per-class IoU results of front-view semantic segmentation on the Stanford2D3D dataset. The average (Avg.) scores are calculated with three folds [2] of cross validation, where Fold-2 is the most challenging split on the Stanford2D3D dataset. Compared to previous state-of-the-art Trans4PASS [39], our proposed 360Mapper achieves 47.97% mIoU in Fold-2 split. Besides, our 360Mapper model has overall better performance (54.34% in mIoU) in the average result calculated by

<sup>2</sup>[https://github.com/atlantia-ar/matterport\\_utils](https://github.com/atlantia-ar/matterport_utils)

three folds evaluation, surpassing the previous Trans4PASS model with +2.24% in mIoU. Furthermore, our model achieves the highest scores in 11 of 13 categories, including *board*, *bookcase*, *ceiling*, *chair*, *clutter*, *door*, *floor*, *sofa*, *table*, *wall*, and *window*. Improvements in these categories demonstrate the effectiveness of our 360Mapper model in combating distortions of 360° front-view images by incorporating distortion-aware 360Attention.

### B.2. Results on 360FV-Matterport

As shown in Table 8, we present the front-view semantic segmentation results on the test set of 360FV-Matterport dataset. We compare our approaches with SegFormer [34], Trans4PASS [39], Trans4PASS+ [40], HoHoNet [29] with RGB and RGB-D, where HoHoNet uses ResNet-101 as backbone and the others use MiT-B2 as backbone. Compared with the well-established existing work SegFormer, our approach obtains a higher mIoU score with 43.16%, having a performance improvement of +0.67% mIoU on the test set. The test set is much more challenging than the validation set of 360FV-Matterport dataset, the results in Table 8 show the superiority of the proposed approach on extracting the underlying cues for the proposed task.

Apart from that, per-class IoU scores on 360FV-Matterport in Table 9. The performance of 360Mapper on both test and validation sets are demonstrated. 360Mapper delivers 46.35% and 43.16% mIoU performance on validation and test sets of 360FV-Matterport dataset respectively. For per-class IoUs, our model has better performance of challenging class, *e.g.*, *sink* with 25.12% and 28.24% on validation and test sets, surpassing Trans4PASS+ [40] with large margins. It notes that the small objects, *e.g.*, *furniture*, *mirror*, *toilet* on the test set, are still challenging for both methods. Apart from these, our models have better semantic segmentation results on 17 of 20 classes on the 360FV-Matterport dataset.

### B.3. Results on 360BEV-Stanford

Per-class IoU scores on 360BEV-Stanford are shown in Table 10. On the 360BEV task, 360Mapper can achieve 45.78% score of mIoU, outperforming the previous Trans4Map [5] method with +9.7%. Specifically, our 360Mapper achieves per-class IoU with 93.33%, 42.52%, 59.14%, 5.06%, 62.66%, 39.75%, 5.48%, 38.74%, 97.76%, 48.92%, 76.76%, 45.86% and 24.89% for *void*, *board*, *bookcase*, *ceiling*, *chair*, *clutter*, *column*, *door*, *floor*, *sofa*, *table*, *wall* and *window*, respectively. Especially, the challenging objects that appear thin lines in bird’s-eye views, such as *doors* and *walls*, can be more stably recognized by our method, which improves both IoUs with 10.23%→38.74% and 29.56%→45.86%. The *beam* class is not successfully recognized by both methods, because this BEV mechanism directly ignores objects on the ceil-

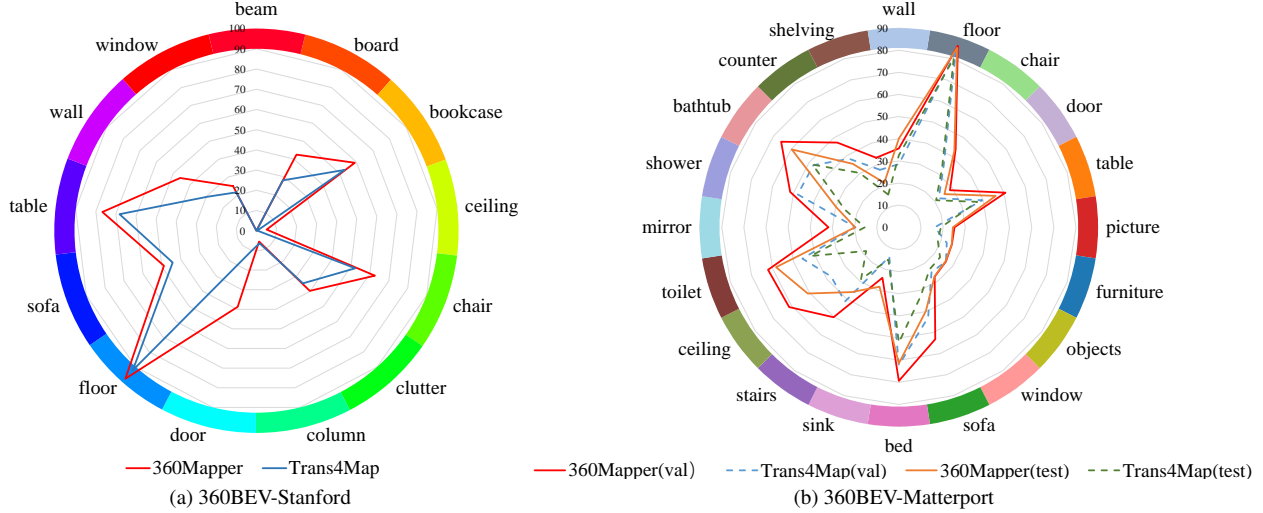


Figure 8. **Distribution of per-class semantic mapping results** (per-class IoU in %) on the 360BEV-Stanford and the 360BEV-Matterport datasets. On the 360BEV-Matterport dataset, the results are compared on respective validation and test sets. Compared to the baseline model Trans4Map [5], our 360Mapper models achieve overall better 360BEV results.

Table 7. **Per-class results (360FV)** on the Stanford2D3D dataset. The models are based on the MiT-B2 [34] backbone.

Method	Split	mIoU	beam	board	bookcase	ceiling	chair	clutter	column	door	floor	sofa	table	wall	window
Trans4PASS [39]	Fold-1	53.30	00.40	69.50	62.20	82.80	58.50	34.30	21.90	44.90	91.20	40.80	57.70	74.80	54.20
Trans4PASS [39]	Fold-2	45.70	12.50	46.90	32.60	82.30	64.70	37.50	20.10	42.70	86.60	17.70	45.20	70.30	35.10
Trans4PASS [39]	Fold-3	57.20	21.40	65.40	58.30	80.20	55.80	41.90	28.60	76.30	88.60	45.40	58.80	59.30	63.60
Trans4PASS [39]	Avg.	52.10	<b>11.40</b>	60.60	51.10	81.80	59.70	37.90	<b>23.50</b>	54.60	88.80	34.60	53.90	68.10	51.00
360Mapper	Fold-1	56.46	00.57	74.61	65.03	83.96	62.41	40.27	18.72	42.22	93.31	53.86	65.90	76.18	58.84
360Mapper	Fold-2	47.97	09.32	41.89	40.45	83.01	62.27	34.92	25.74	57.74	88.02	24.48	42.95	72.19	41.22
360Mapper	Fold-3	58.60	08.05	74.32	61.05	81.05	63.29	44.44	4.64	76.56	90.91	57.28	62.52	64.96	72.77
360Mapper	Avg.	<b>54.34</b>	05.98	<b>63.61</b>	<b>55.51</b>	<b>82.67</b>	<b>62.66</b>	<b>39.88</b>	16.37	<b>58.84</b>	<b>90.75</b>	<b>45.21</b>	<b>57.12</b>	<b>71.11</b>	<b>57.61</b>

Table 8. **Panoramic semantic segmentation (360FV)** on the test set of 360FV-Matterport dataset.

Method	Backbone	Input	mIoU(%)
HoHoNet [29]	ResNet-101	RGB	40.22
HoHoNet [29]	ResNet-101	RGB-D	41.23
Trans4PASS [39]	MiT-B2	RGB	39.70
Trans4PASS+ [40]	MiT-B2	RGB	40.41
SegFormer [34]	MiT-B2	RGB	42.49
Ours	MiT-B2	RGB	<b>43.16</b>

ing. Different from the front-view semantic segmentation task, the *void* class is included on the 360BEV task, because this class can be used to indicate the invisible area on the BEV semantic maps, which is important for the downstream task, such as path planing. Based on the per-class scores

shown in Figure 8a, 360Mapper shows overall promising performance on the presented 360BEV-Stanford dataset, indicating the effectiveness of our methods in addressing the 360BEV task.

#### B.4. Results on 360BEV-Matterport

The 360BEV results on the test set of 360BEV-Matterport are demonstrated in Table 11. We further compare our approach with three backbones, *e.g.*, MiT-B0, MiT-B2 from SegFormer [34] and MSCA-B from SegNeXt [11] on the test set of the 360BEV-Matterport for the panoramic semantic mapping task. Methods based on intermediate projection show the most promising results compared with those based on early projection and late projection. The result is consistent compared with the ones demonstrated on the validation set of 360BEV-Matterport dataset. 360Map-



Table 9. **Per-class results (360FV)** on the 360FV-Matterport dataset.

Method	Backbone	Data	mIoU	wall	floor	chair	door	table	picture	furniture	objects	window	sofa	bed	sink	stairs	ceiling	toilet	mirror	shower	bathub	counter	shelving
Trans4PASS+ [40]	MiT-B2	val	42.60	63.37	79.11	39.13	40.31	32.76	35.99	30.96	31.52	37.52	44.01	63.17	20.60	41.76	77.55	40.71	24.27	23.73	58.34	34.31	32.90
360Mapper	MiT-B2	val	<b>46.35</b>	64.12	83.14	45.75	44.98	37.96	41.08	32.26	35.07	40.61	48.69	69.80	25.12	47.80	80.15	45.96	28.70	22.31	60.05	38.64	34.82
Trans4PASS+ [40]	MiT-B2	test	40.41	64.32	80.12	41.24	41.70	30.86	36.93	35.16	28.27	32.65	33.28	55.98	22.93	37.19	78.36	48.96	17.73	26.51	49.65	28.64	22.82
360Mapper	MiT-B2	test	<b>43.16</b>	66.95	82.24	45.12	47.34	32.72	44.35	33.34	29.57	34.59	32.08	62.06	28.24	38.03	81.26	45.47	23.61	29.01	55.44	28.58	23.24

Table 10. **Per-class results (360BEV)** on the 360BEV-Stanford2D3D dataset.

Method	Backbone	mIoU	void	beam	board	bookcase	ceiling	chair	clutter	column	door	floor	sofa	table	wall	window
Trans4Map [5]	MiT-B2	36.08	64.17	0.00	28.10	52.96	0.45	52.30	34.71	6.40	10.23	92.18	44.29	68.22	29.56	21.44
360Mapper	MiT-B2	<b>45.78</b>	93.33	0.00	42.52	59.14	5.06	62.66	39.75	5.48	38.74	97.76	48.92	76.76	45.86	24.89

Table 11. **Panoramic semantic mapping (360BEV)** on the test set of 360BEV-Matterport dataset.

Method	Backbone	Acc	mRecall	mPrecision	mIoU
(1) Early projection: Proj. → Enc. → Seg.					
SegFormer [34]	MiT-B2	69.72	35.28	40.41	24.04
SegNeXt [11]	MSCA-B	69.99	36.25	41.96	25.22
(2) Late projection: Enc. → Seg. → Proj.					
HoHoNet [29]	ResNet101	62.89	35.18	39.54	22.01
Trans4PASS [39]	MiT-B2	53.50	29.35	33.53	16.53
Trans4PASS+ [40]	MiT-B2	57.24	30.639	34.49	17.72
SegFormer [34]	MiT-B2	62.91	35.35	39.64	22.02
(3) Intermediate projection: Enc. → Proj. → Seg.					
BEVFormer [16]	MiT-B2	72.04	36.69	47.90	27.46
Trans4Map [5]	MiT-B0	71.78	38.27	43.77	26.52
Trans4Map [5]	MiT-B2	72.94	45.45	47.03	31.08
Trans4Map [5]	MiT-B4	73.60	44.33	49.91	31.79
Ours	MiT-B0	76.02	43.11	50.41	31.35 (+4.83)
Ours	MiT-B2	78.04	54.47	54.27	38.78 (+7.70)
Ours	MSCA-B	79.17	55.16	57.27	40.27

per still delivers the state-of-the-art results for the proposed 360BEV task on the test set, indicating the effectiveness of the proposed architecture. Especially, our 360Mapper with MiT-B2 backbone (38.78%) can surpass Trans4Map with MiT-B2 (31.08%) as well as the one with MiT-B4 (31.79%). Besides, the proposed method based on MSCA-B backbone achieves the best result with 40.27% in mIoU.

Per-class IoU scores on the 360BEV-Matterport dataset are presented in Table 12. The performance of 360Mapper under MiT-B2 from SegFormer [34] and MSCA-B from SegNeXt [11] are included, which achieves promising performance for the 360BEV task. Compared to Trans4Map [5], our 360Mapper with the same MiT-B2 backbone can achieve respective 44.32% and 38.78% in mIoU on the validation set and the test set. The *void* class is

also included on the 360BEV-Matterport dataset. From the Figure 8b presented, it is readily apparent that our model can better recognize the *chairs* and *tables* on the bird’s-eye-view semantic maps, yielding more than 6% IoU gains compared to Trans4Map [5]. On the test set, 360Mapper with MiT-B2 obtain IoU gains with >12% and >15% on the *sink* and *toilet* classes, as compared to Trans4Map. Besides, if using a stronger backbone, e.g., MSCA-B [11], our proposed methods can achieve higher semantic mapping results on both of validation and test sets of 360BEV-Matterport dataset, which are 46.31% and 40.27% in mIoU, respectively.

## C. More Qualitative Analysis

### C.1. Analysis on Stanford2D3D

The visualization of front-view semantic segmentation (360FV) on the Stanford2D3D dataset is shown in Fig. 9, where the RGB input, the prediction of the baseline, the prediction of our model and the ground truth are depicted from left to the right. The corresponding color map is showcased at the top of Fig. 9. Compared with the baseline Trans4Pass [39], the panoramic semantic segmentation results of our model have clear boundaries among different objects which is much more similar to the ground truth, e.g., the *door* and the *clutter* of the second sample. Our method also show promising performance on the objects with small spatial size, e.g., *chairs*, compared with the baseline in the last sample, indicating that our 360Attention approach is good at grasping underlying context feature and cues through the deformable sampling locations.

### C.2. Analysis on 360FV-Matterport

Fig. 10 is the front-view semantic segmentation visualization of the presented 360FV-Matterport dataset, providing a detailed depiction of the spatial distribution of differ-

Table 12. **Per-class results (360BEV)** on the 360BEV-Matterport dataset.

Method	Backbone	Data	mIoU	void	wall	floor	chair	door	table	picture	furniture	objects	window	sofa	bed	sink	stairs	ceiling	toilet	mirror	shower	bathub	counter	shelving
Trans4Map [5]	MiT-B2	val	36.72	47.87	28.52	82.96	34.44	22.27	39.58	16.28	22.75	26.29	25.08	42.81	62.25	13.95	41.51	37.79	45.82	19.56	48.05	47.71	38.25	27.31
360Mapper	MiT-B2	val	44.32	74.30	31.94	85.85	42.01	26.71	46.40	23.21	25.00	24.87	27.36	51.37	66.59	20.99	47.07	54.97	56.91	29.50	55.70	63.16	45.82	31.04
360Mapper	MSCA-B	val	<b>46.31</b>	74.43	35.62	86.17	43.60	28.56	50.61	25.11	25.17	26.26	27.56	53.17	69.36	24.02	50.24	61.26	62.11	31.77	51.60	65.71	47.32	33.06
Trans4Map [5]	MiT-B2	test	31.08	40.51	32.54	80.21	33.23	20.85	37.21	19.01	18.46	23.05	23.56	32.35	52.08	15.34	29.02	18.27	41.90	15.39	25.58	48.19	30.38	15.52
360Mapper	MiT-B2	test	38.78	60.36	36.77	84.34	39.93	24.41	44.58	25.23	21.97	25.20	27.06	36.59	60.84	28.46	35.60	49.69	57.39	19.35	25.84	56.91	37.23	16.60
360Mapper	MSCA-B	test	<b>40.27</b>	62.82	40.09	85.22	42.60	25.48	46.00	24.37	25.11	26.08	27.39	39.68	61.45	28.18	36.17	50.88	58.31	19.77	29.85	59.78	35.39	21.14

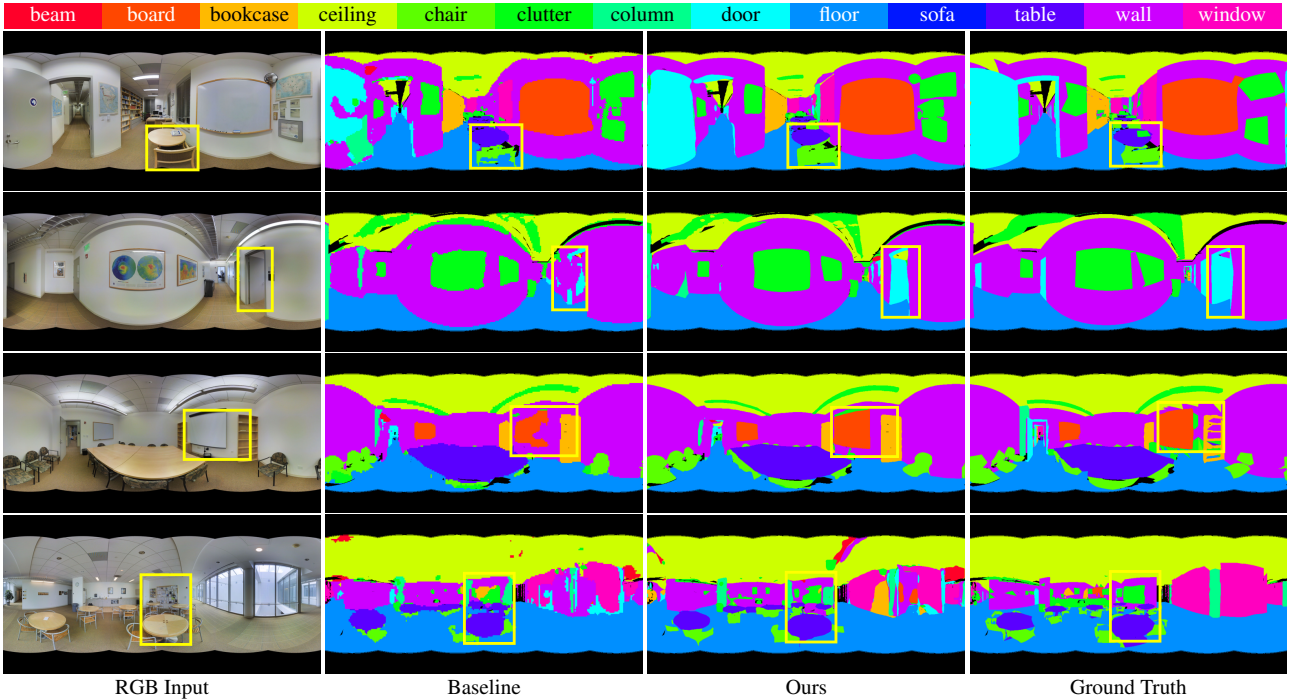


Figure 9. **360FV visualization and qualitative analysis** on the Stanford2D3D dataset.

ent semantic classes. Compared with the baseline method Trans4Pass [39], our model produces segmentation results exhibit more precise contours and clearer boundaries between different objects, which closely resemble the ground truth segmentation labels, *e.g.*, the *toilet* and the *door* of the first sample. In the second row, the *door* on the right side is not recognized by the baseline model. In contrast to the baseline method, our model is able to accurately distinguish the *door* class from its surrounding *object* and *wall* classes, despite its small size and low contrast with the surrounding environment. The *table* in the center of the third sample are correctly predicted by our model while it is erroneously segmented by the baseline as *furniture*. This highlights the superior performance of 360Mapper in panoramic semantic segmentation under challenging conditions. In the last two rows, the small *chair* by the wall and the *door* are correctly recognized by our model.

### C.3. Analysis on 360BEV-Stanford

We further introduce the qualitative results of 360BEV task on the 360BEV-Stanford dataset in Fig. 11. The RGB input, the BEV semantic mapping results of the baseline and 360 Mapper, the BEV semantic mapping ground truth are depicted from left to right, where the color map is shown at the top of Fig. 11. The *chairs* of the first and the second sample are correctly predicted by our method while they are partially or entirely missed by the baseline. Compared with the 360Mapper, the baseline shows more false prediction especially regarding some furniture, *e.g.*, the false predicted *bookcase* at the third sample, which should be predicted as *chairs*. At the last row of Fig. 11, the challenging *door* is not recognized by the baseline model, while our 360Mapper can provide accurate *door* segmentation result, even it is a thin line in the BEV map. Our method shows overall su-



Figure 10. **360FV visualization and qualitative analysis** on the 360FV-Matterport dataset.

terior performance on the proposed task compared with the baseline in terms of the semantic segmentation performance on small objects, which further illustrates the strength by using 360Attention.

#### C.4. Analysis on 360BEV-Matterport

Fig. 12 presents qualitative results for the 360BEV task on the 360BEV-Matterport dataset. We observe that our 360Mapper outperforms the baseline method Trans4Map [5] in terms of accurately segmenting small objects. In particular, the baseline method exhibits more false predictions, such as the misclassified *chair* in the first sample and *object* misidentified as *table* in the second sample. Surprisingly, the different steps of *stairs* in the third and the fourth sample are recognized correctly by both methods. However, we find the fifth sample to be particularly challenging, as both the baseline and our 360Mapper recognize the object in the center of the image as a *counter*, which is a *table* as shown in the ground truth. This failure case shows the difficulty of accurately distinguishing between similar object categories from the context of panoramic images to the bird’s-eye-view semantic maps.

#### D. Acknowledgments

This work was supported in part by Helmholtz Association of German Research Centers, in part by the Ministry of Science, Research and the Arts of Baden-Württemberg (MWK) through the Cooperative Graduate School Accessibility through AI-based Assistive Technology (KATE) under Grant BW6-03, in part by the University of Excellence through the “KIT Future Fields” project, in part by Hangzhou SurImage Technology Company Ltd., and in part by the Helmholtz Association Initiative and Networking Fund on the HAICORE@KIT partition. This work was partially performed on the HoreKa supercomputer funded by the MWK and by the Federal Ministry of Education and Research.

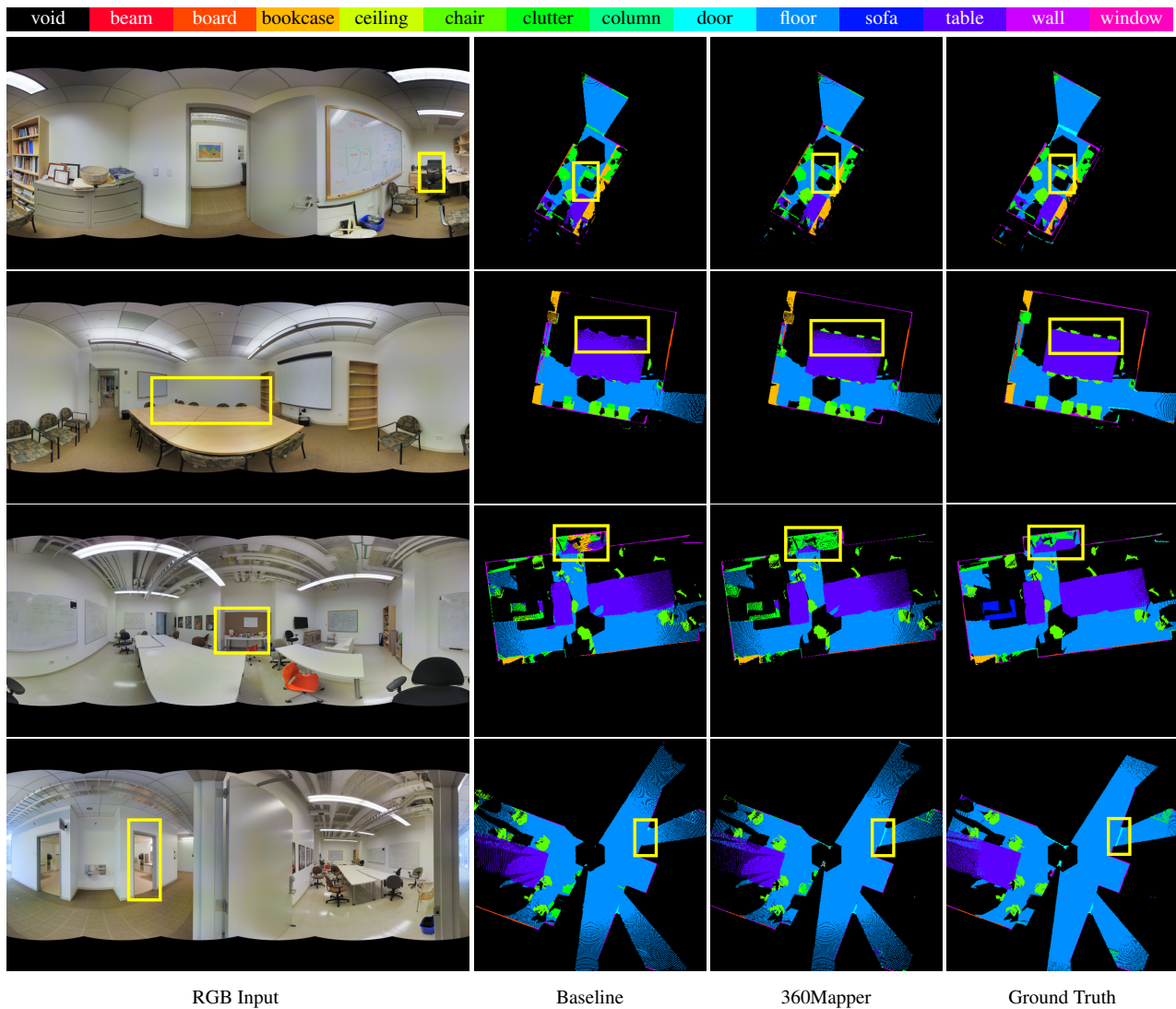


Figure 11. **360BEV visualization and qualitative analysis** on the 360BEV-Stanford dataset. Black regions are the `void` class, indicating the invisible areas in BEV semantic maps. Zoom in for better view.



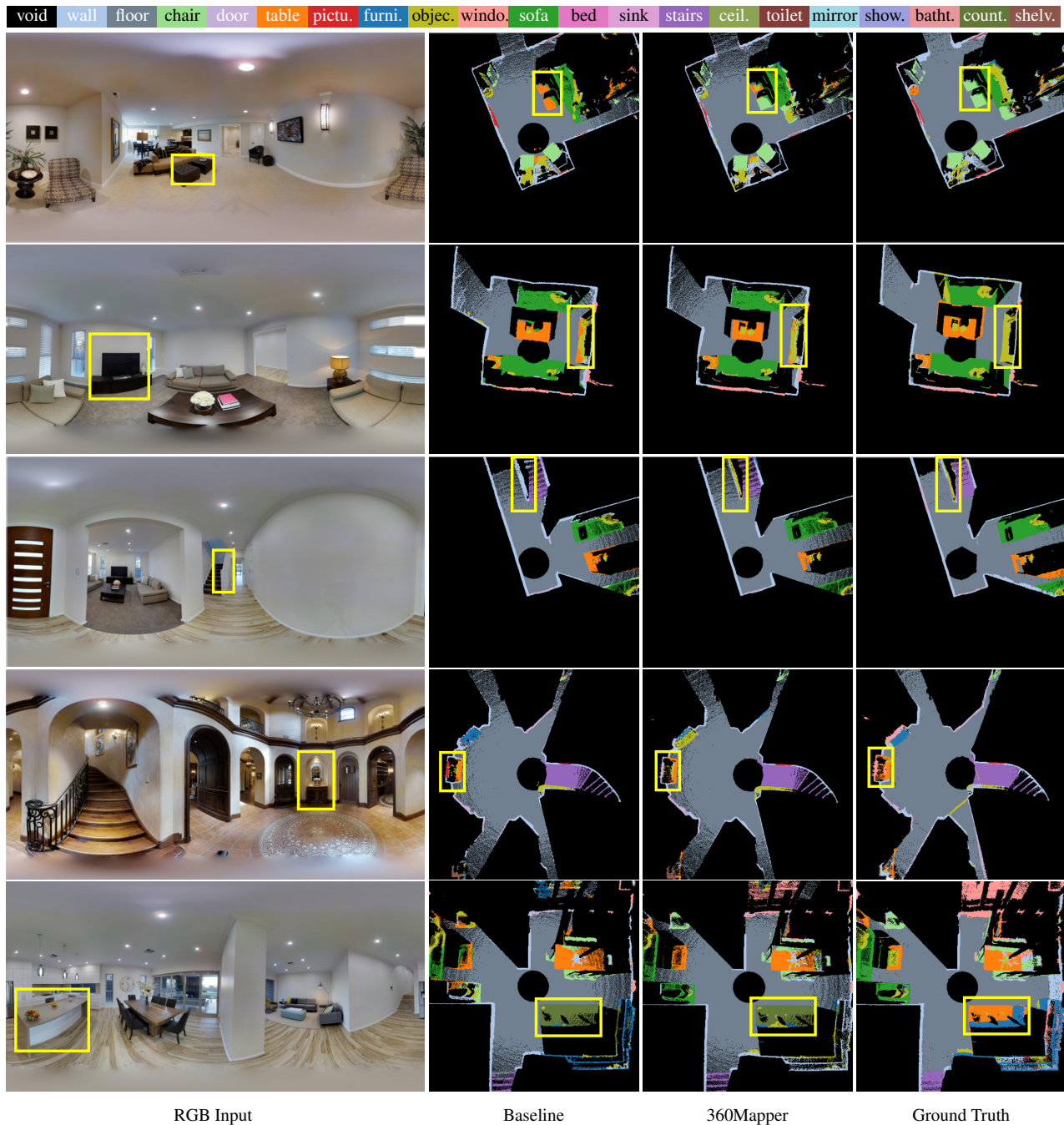


Figure 12. **360BEV visualization and qualitative analysis** on the 360BEV-Matterport dataset. Black regions are the `void` class, indicating the invisible areas in BEV semantic maps. Zoom in for better view.